Ultrasonic wave transport in strongly scattering media

J. H. Page

Department of Physics and Astronomy
University of Manitoba
Winnipeg, MB Canada R3T 2N2

Summary. — Ultrasonic experiments are well suited to the investigation of classical wave transport through strongly scattering media, and are playing a role that is often complementary to investigations using light or microwaves. Advantages of ultrasonic techniques are their ability to readily detect the wave field (not just the intensity), to perform experiments resolved in both time and space, and to control the properties of the medium being investigated over a wide range of scattering contrasts. This first paper reviews what has been learned from ultrasonic experiments over the last 15 years about the ballistic and diffusive propagation of classical waves through strongly scattering disordered media. These results are compared with studies of ordered media (phononic crystals), where band gaps and super-resolution focusing have been observed.

(*) Published in the Proceedings of the International School of Physics Enrico Fermi, Course CLXXIII, "Nano Optics and Atomics: Transport of Light and Matter Waves", edited by R. Kaiser, D.S. Weirsma and L. Fallani (IOS, Amsterdam; SIF, Bologna, 2011) pp. 75-93. The original publication is available from SIF at http://www.sif.it/SIF/en/portal/books/series/rendiconti_fermi.

1. – Introduction

For more than a decade, there has been growing interest in ultrasonic wave transport in strongly scattering media. Just as for other classical waves, such as light and microwaves, much of this interest revolves around the many unusual wave phenomena have been observed at intermediate frequencies, where the wavelengths are comparable to the size of the scatterers [1]. Examples range from strikingly large variations in wave speeds caused by strong resonant scattering (when a pulse can even appear to travel so quickly through a sample that its velocity is negative) to the inhibition of wave propagation that can occur in very strongly scattering samples when the waves become localized. In seeking to discover and understand such wave phenomena, ultrasonic experiments have an important role to play, partly because of the relative ease with which the full wave field, rather than just the intensity, can be measured. Thus, ultrasonic techniques give direct experimental access to the wave function and/or Green's function, allowing both phase and amplitude information to be obtained. Ultrasound is also well adapted to pulsed experiments, enabling the path length dependence of the transmission or reflection to be resolved in time, usually in the near field. Furthermore, the fact that the scattering contrast is governed by differences in both velocity and density enables the scattering strength to be controlled over a very wide range. As a result, experiments with acoustic or elastic waves can make important contributions to both fundamental studies and practical applications of wave scattering in complex media, and are often complementary to optical and microwave methods for investigating these phenomena.

In this paper, I will review the progress that has been achieved over the last 15 years in understanding how ultrasonic waves propagate through both random and ordered media. The regime of interest here is one where multiple scattering dominates, but the scattering is not so strong that the interference effects leading to Anderson localization are present. (The latter is the subject of the second paper in this series, while the third paper discusses applications such as Diffusing Acoustic Wave Spectroscopy.) To illustrate the scope of information that is accessible to ultrasonic experiments in random systems, section **2** summarizes results obtained for acoustic waves (longitudinal polarization only) in a model system consisting of a suspension of glass beads in a liquid, where a rather complete picture of wave transport has been achieved through transmission measurements. Other types of acoustic scattering systems (plastic spheres and bubbles surrounded by water), which lead to different wave behaviour, are also mentioned. By contrast to the diffusive transport of energy that is seen in disordered systems, the propagation of multiply scattered waves in ordered media is characterized by a coherent multiply scattered wave field, leading to band gaps and unusual focusing phenomena. These effects are described in the last major section of the paper on phononic crystals (section **3**).

2. – Acoustic wave transport in random media

Many features of ultrasound transport in strongly scattering media are demonstrated by acoustic pulse propagation experiments that have been performed in a disordered

medium consisting of randomly packed 0.5-mm-radius glass beads immersed in water [2, 3, 4, 5]. Strong scattering in this model system is ensured by the large acoustic impedance difference between glass and water ($Z_{glass}/Z_{water} \approx 10$, where $Z{=}\rho v_p$ is the acoustic impedance, ρ is the density and v_p is the phase velocity). Although the transmitted signals are dominated by multiply scattered waves at intermediate frequencies, the phase sensitivity of piezoelectric ultrasonic transducers allows measurements to be made of the weak signal that propagates ballistically through the medium without scattering out of the forward direction. This ballistic signal remains coherent both temporarily and spatially with the input pulse, so that it can be extracted by averaging the transmitted wave field over many speckles, a procedure that causes the multiply scattered component to cancel because of the random phase fluctuations from speckle to speckle. The separation of the ballistic pulse from the multiply scattered waves, whose energy transport was found to be well described by the diffusion approximation, allows a very complete picture of wave transport in strongly scattering media to be obtained.

2˙1. *Ballistic propagation.* – Figure 1 shows an example of how the ballistic pulse can be extracted from the total transmitted field when the sample is sufficiently thin. The experiments were performed by enclosing the suspension of glass particles in a cell with thin walls that are transparent to ultrasound, and then placing the sample in a water tank between a plane-wave generating transducer and a subwavelength-diameter hydrophone detector. The hydrophone position was scanned in a plane near the surface of the sample to measure the transmitted signal in many independent coherence areas, or speckles, using a grid separation of approximately a wavelength. The wave field averaged over more than 100 speckles reveals the ballistic pulse, shown by the solid curve in fig. 1(b). The multiply scattered waveforms (fig. 1(c)), often called the coda, especially in the context of seismic waves, since they arrive after the ballistic pulse, can then also be obtained by subtracting the ballistic pulse from the total transmitted field in each speckle. This demonstration of coherent ballistic pulse propagation provides convincing experimental evidence that a (uniform) effective medium can still be defined in the intermediate strongly scattering regime, a result that has been inferred less directly in recent optical experiments [6].

The ballistic pulse contains information that is crucial for determining the frequency dependence of the scattering properties of any sample, as it allows both the phase and group velocities [$v_p = \omega/k$, $v_g = d\omega/dk$] as well as the scattering mean free path l_s [$I(L) = I(0)\exp(-L/l_s)$], to be determined [5]. Here ω, k, L and I are the angular frequency, wave vector, sample thickness and ultrasound intensity, respectively. Experimentally, v_p and l_s are determined from the phase difference $\Delta\phi$ and amplitude ratio $A(L)/A(0)$ of the fast Fourier transforms (FFT) of the ballistic and input pulses ($v_p = \omega L/\Delta\phi$, $l_s = -L/\ln[A(L)/A(0)]^2$). The group velocity is accurately measured by digitally filtering the ballistic and input pulses using a narrow Gaussian filter, whose bandwidth is chosen to be sufficiently narrow that pulse distortion due to dispersion is negligible, and measuring the delay t_g between their peak arrival times ($v_g = L/t_g$).

Results for randomly close packed suspensions of glass beads in water are shown in

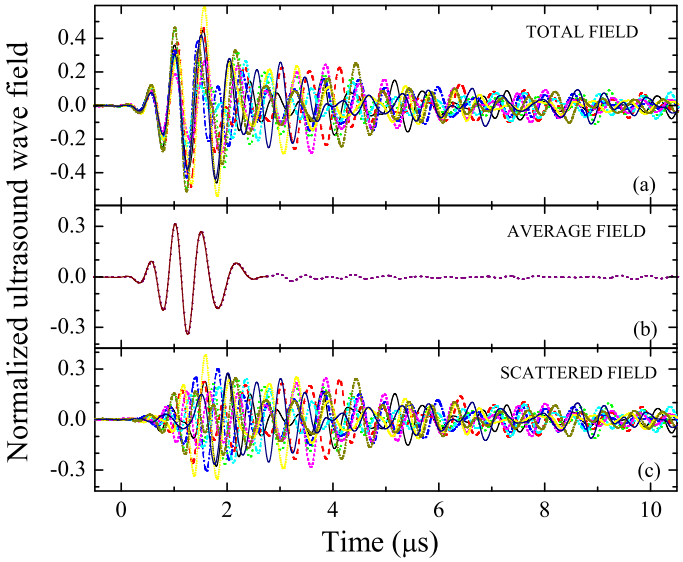

Fig. 1. – Comparison of the total field (a), average field (b) and scattered field (c) transmitted through a thin sample (thickness, $L = 1.7$ mm) of glass spheres in water. The data are normalized with respect to an input pulse of unit peak amplitude.

fig. 2 over a wide frequency range, corresponding to wavelengths from approximately $5a$ to $0.5a$ (dimensionless frequency range: $1 \lesssim k_w a \lesssim 10$, where k_w is the wavelength in water and a is the bead radius). For $k_w a > 2$, strongly scattering is seen, with the scattering mean free path approaching the bead radius, and the product kl_s ranging from 3 to 9. Both the phase and group velocities exhibit a considerable frequency dependence, with the group velocity varying by more than a factor of 2. Note the very low values of the group velocity near $k_w a = 2$, where v_g is substantially less than the sound velocities in either water or glass ($v_w = 1.5$ mm/μs, $v_{glass} = 5.6$ or 3.4 mm/μs for longitudinal or transverse polarizations).

The origin of these large velocity variations can be understood using an effective medium model, based on a Spectral Function Approach (SpFA), which overcomes a fundamental limitation of the traditional Coherent Potential Approximation (CPA) in the intermediate frequency regime [3]. The scattering is calculated by modeling a typical glass bead scatterer as an elastic sphere that is coated with a layer of water and embedded in a homogeneous effective medium, which accounts for the presence of all the other scatterers. The dispersion relation, ω versus k, for acoustic waves in the medium is then determined by identifying the peaks of the spectral function, given by the negative imaginary part of the Green's function. The simple physical interpretation of the method is that these peaks correspond to the locus of points in the frequency-wavevector plane where the scattering is weakest, so that they delineate the modes that succeed in propagating through the

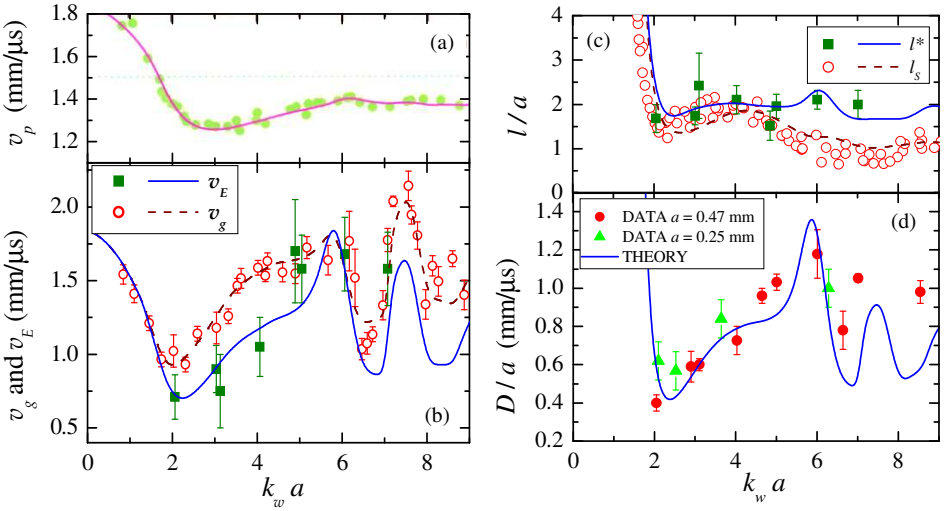

Fig. 2. – Frequency dependence of (a) the phase velocity, (b) the group and energy velocities, (c) the scattering and transport mean free paths, and (d) the diffusion coefficient. The dotted horizontal line in (a) indicates the sound velocity in water. All data (symbols) and theory (solid and dashed curves) were measured/averaged over a small 5% variation in the bead size.

medium and identify the effective medium properties. The approach is accurate so long as $kl_s \gtrsim 2$ [5]. This dispersion relation enables v_p and v_g to be calculated, giving the excellent agreement with the experimental data shown in fig. 2. In addition, the scattering mean free path can be determined from the scattering cross section of the coated elastic sphere [3, 5]. By calculating the energy density of a typical scatter as a function of frequency, the sharp features in the group velocity near $k_w a \sim 2$ and above $k_w a \sim 5$ were found to be associated with resonances of the fluid coating and solid spheres, respectively, leading in the first case to a slowing down of the velocity by tortuosity of the connected fluid pathways and in the second case to resonant trapping of energy in the solid scatterers [5]. The overall mechanism underlying the frequency dependence of the phase and group velocities can be understood as follows: because of the strong coupling between the resonant scatterers, the uniform effective medium sensed by the coherent ballistic propagation is very strongly renormalized, in much the same way as quantum mechanical resonances are shifted when there is strong coupling between them. Thus, the ballistic pulse is still able to propagate coherently while being very strongly affected by the scatterers. These experimental and theoretical results also show that the group velocity remains well defined despite the strong scattering [3], thereby addressing a question about the meaning of the group velocity in dispersive media that was raised by Sommerfeld [7] and Brillouin [8] in the first part of the 20th century and discussed more recently by Albada *et al.* [9].

Ultrasonic experiments on other types of suspensions with different acoustic properties have also been performed to examine how ballistic pulse propagation is affected by the

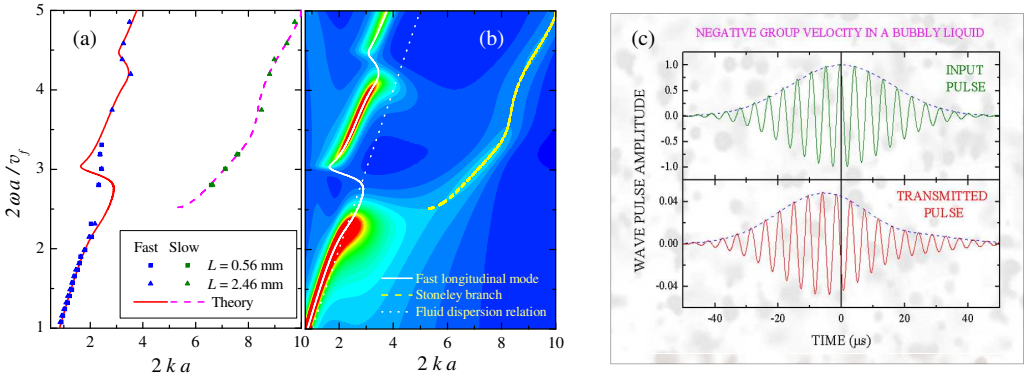

Fig. 3. – (a), (b) Dispersion curves for a suspension of PMMA spheres in water. In (a), experimental results are represented by symbols for two different sample thicknesses, and theoretical predictions from the peaks of the spectral function (shown in (b)) are shown by the solid curves. (c) Incident and transmitted pulses through a cloud of bubbles, which are shown in the grey scale background picture behind the graphs. The bubbles were generated by an electrolysis method and had a radius of ~ 15 μm.

strength and character of the scattering resonances. One interesting example is a slurry of randomly close packed plastic spheres in water, where gaps open up in the mode spectrum due to scattering resonances having the character of interfacial or Stoneley waves. These Stoneley-wave-like resonances involve both longitudinal and transverse displacements inside the spheres, and compressional deformations of the surrounding nearby liquid. As a result, a second longitudinal mode with slow velocities, due to the coupling between these Stoneley wave resonances on adjacent spheres, is observed. This slow mode was first discovered by Brillouin scattering experiments [10], which probe the modes of the system by measuring the frequencies of the modes at fixed wave vector, in contrast to ultrasonic pulse propagation experiments, which measure the velocities of the modes at fixed frequency. Ultrasonic measurements of the dispersion relations are shown in fig. 3(a), and compared with peaks in the spectral function (fig. 3(b)) predicted by the SpFA model. Good overall agreement is found, confirming the basic character of the unusual modes of this system. In contrast to the Brillouin scattering results, the ultrasonic measurements reveal that because of absorption, longitudinal modes still propagate inside the "gap" and interfere with the Stoneley wave branch, leading to rich behaviour that provides a stringent test of the accuracy of the SpFA model.

A second example of the effects of very strong scattering is acoustic pulse propagation through a suspension of bubbles. The acoustic properties of bubbly suspensions are dominated by a low-frequency multipole resonance, leading to a wide range of unusual wave phenomena such as anomalous dispersion and superradiance (e.g., see refs. [11, 12, 13]). One remarkable consequence is shown in fig. 3(c), which provides compelling experimental evidence that the group velocity is negative near the fundamental bubble resonance frequency [14]. This unusual effect occurs because of pulse reshaping due to the

anomalous dispersion, which leads to constructive interference at the leading edge of the pulse and destructive interference at the trailing edge; thus, the peak of the transmitted pulse emerges from the sample before the peak of the input pulse has entered it, so that the pulse transit time and hence group velocity is negative. It is noted that, at a given time, the intensity of the incident wave is always greater than the transmitted one, so that causality is not violated. In this case and in analogous examples for light [15], the group velocity still accurately describes ballistic pulse propagation, providing the bandwidth is sufficiently narrow, but can no longer correspond to the ballistic energy transport velocity [16].

2˙2. *Diffusive propagation.* – Transport beyond the scale of the mean free path is dominated by multiply scattered waves (fig. 1(c)). So long as the thickness of the sample is greater than about three mean free paths and the scattering is not so strong that $kl_s \sim 1$, the transport of energy in ultrasonic experiments is well described using the diffusion approximation [2, 17]. In this approximation, all phase information is ignored and the quantity of interest is energy transport, which is treated as a random walk process, characterized by the diffusion coefficient $D = v_E l^*/3$. Here v_E is the average local velocity of energy transport, and l^* is the transport mean free path, or distance over which the direction of propagation is randomized. The transport and scattering mean free paths are related by $l^* = l_s/(1-\langle\cos\theta\rangle)$, where θ is the scattering angle, and are therefore equal only when the scattering is isotropic. Dynamic (pulsed) measurements, which probe the distribution of multiply scattered path lengths in the time domain, are sensitive to D, while steady state (continuous wave) experiments, such as the measurement of total energy transmission, are sensitive to l^*/L.

To demonstrate the applicability of the diffusion approximation to acoustic wave transport in strongly scattering media, and to measure D, l^* and v_E over a wide frequency range, an extensive series of pulsed and quasi-continuous-wave experiments have been performed on the same glass bead suspensions described above [2, 4, 17]. For examples of other approaches to investigating diffusive transport of acoustic waves in 3D and 2D systems, see references [18, 19]. In refs. [2, 4, 17], slab-shaped samples were used and the diffusion coefficient was measured from the temporal evolution of the average transmitted intensity, $I(t)$, which was determined by averaging the square of the envelope of the scattered sound field over a large number of independent speckles. Typical results, which were obtained using a tightly focused incident pulse to create a point source, are shown in fig. 4(a) for three different sample thicknesses, ranging from 7 to 30 scattering mean free paths. Comparison of the experimental data with solutions of the diffusion equation was facilitated by performing the measurements on slab-shaped samples, with widths at least 10 times the thickness so that edge effects could be ignored (i.e., the samples were excellent approximations to infinite slabs for the range of times over which signals could be detected). Accounting for internal reflections at the front and back faces of the slab and the possibility of dissipation inside the sample, the transmitted intensity (flux) for a delta function diffuse source of unit strength in time and position, $\delta(t)\delta(x-x')\delta(y-y')\delta(z-z')$, is given by the solution of the diffusion equation with these

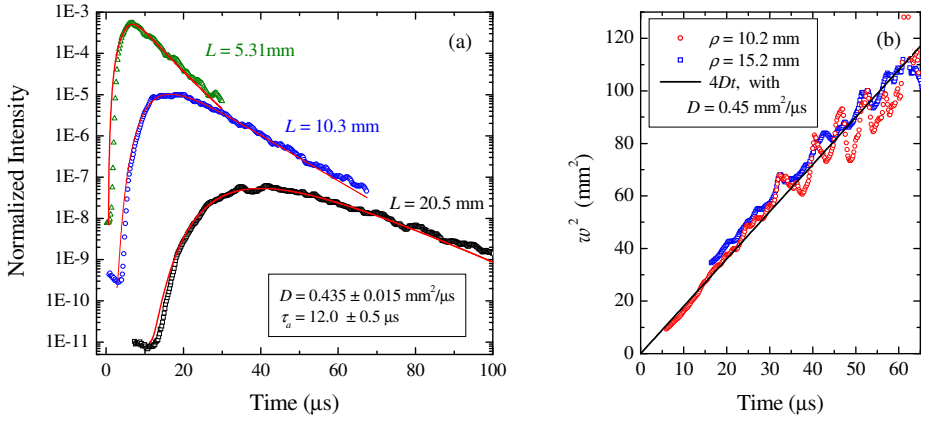

Fig. 4. – (a) Time dependence of the transmitted intensity, normalized so that the peak of the corresponding input pulse is unity, for three randomly close-packed glass-bead-in-water samples having different thicknesses L. The symbols represent experimental data taken with a point source, and the solid curves are fits to the predictions of the diffusion approximation, from which the diffusion coefficient and absorption time are determined. (b) Time dependence of the mean square transverse width w^2 of the diffuse halo for a slab shaped sample. The linear growth of w^2 is characteristic of a diffusion process, enabling D to be measured from the slope of the straight line fit (solid line) independent of absorption and boundary conditions.

boundary conditions:

$$I(t) = -D\left.\frac{\partial U}{\partial z}\right|_{z=L} = \frac{e^{-\rho^2/4Dt}e^{-t/\tau_a}}{2\pi L^2 t}\sum_{n=1}^{\infty} A_n e^{-D\beta_n^2 t/L^2} \tag{1}$$

where τ_a is the absorption time, β_m are the positive roots of the transcendental equation $\tan\beta = 2\beta K/(\beta^2K^2 - 1)$, K is equal to z_0/L with $z_0 = (2l^*/3)(1 + R)/(1 - R)$ (z_0 is known as the extrapolation length, since it is the distance outside the sample where the diffuse energy extrapolates to zero), R is the angle-averaged reflectivity of diffuse sound at the sample boundaries (calculated from the acoustic impedance mismatch), and the coefficients A_n are given by an analytic function of β_n, K and z' [2]. Here $\rho = \sqrt{(x - x')^2 + (y - y')^2}$ is the transverse distance in the plane parallel to the slab at which the intensity is detected relative to the point directly opposite the source. The location of the diffuse source inside the sample, z', has been shown by numerical simulations to be equal to l^* [20]. The solid curves in fig. 4(a) show the results of least squares fits of eq. (1) to this data set, with the initial increase of $I(t)$ being sensitive to D and the tail quite strongly influenced by τ_a. The good agreement between theory and experiment demonstrates the validity of the diffusion approximation for multiply scattered sound, enabling reliable measurements of both D and τ_a to be made.

One advantage of the point source geometry is that it enables the growth of the

diffuse halo to be measured in the transverse direction parallel to the surface of the slab. This gives a method of measuring D directly, independent of boundary conditions and absorption [2]. Experimentally, the average transmitted intensity at transverse distance ρ ("off-axis") and at $\rho = 0$ ("on-axis") are measured by averaging over different sample positions with source and detector positions fixed relative to each other. From eq. (1), it can be seen that the ratio $I(\rho,t)/I(0,t)$ is given simply by $e^{-\rho^2/4Dt} = e^{-\rho^2/w^2(t)}$, so that the the transverse width $w(t)$ of the diffuse halo grows as the square root of time, as expected for a diffuse process. Plotting $w^2(t)$ versus time enables D to be measured from the slope of a straight line fit to the data, as shown in fig. 4(b). The excellent agreement between the values of D measured directly from the transverse width, and from the more cumbersome fits of eq. (1) to the time of flight profile, gives additional confidence in the accuracy with which the diffusion coefficient can be measured in pulsed transmission measurements.

Ultrasonic experiments can also be performed using a good approximation to a plane wave source by placing the sample in the far field of a planar immersion transducer. The solution of the diffusion equation for this experimental geometry can be obtained by integrating eq. (1) over x' and y', giving $I_{\text{plane}}(t) = 4DtI_{\text{point}}(\rho = 0, t)$. Again, accurate measurements of D can be obtained by fitting this expression to the measured time-of-flight profiles for this geometry (e.g., see ref. [2]). This exact solution of the diffusion equation is often approximated by the somewhat simpler expression

$$U(t) \approx \frac{2e^{-t/\tau_a}}{\pi(L+2z_0)} \sum_{n=1}^{\infty} e^{-Dn^2\pi^2 t/(L+2z_0)^2} \sin\left(\frac{n\pi(z\ +z_0)}{L+2z_0}\right) \sin\left(\frac{n\pi(z'+z_0)}{L+2z_0}\right) \tag{2}$$

Equation (2) is a good approximation in many experimental situations, especially at long times, but is not accurate for large values of the reflectivity R. At long times, in the absence of absorption, eq. (2) is proportional to $\exp -t/\tau_D$, with $\tau_D = (L+2z_0)^2/(\pi^2 D)$. This gives a very simple result for the exponential decay of the time of flight profile in terms of the diffusion time τ_D, which is determined by the effective thickness of the sample $L + 2z_0$ and the diffusion coefficient.

Results for the frequency dependence of the diffusion coefficient in the glass bead suspensions are shown in fig. 2(d). A considerable variation, roughly a factor 3, is seen over the range of frequencies investigated. To determine its origin, experiments were also performed for very long pulses to attain quasi-continuous-wave conditions, so that l^* could be measured from the thickness dependence of the total transmitted intensity, $I(L) = \text{fn}(l^*/L, \alpha = \sqrt{D\tau_a})$ (see ref. [2] for the complete expression). It was found that l^* has at most a very weak frequency dependence (fig. 2(c)), being approximately equal to the diameter of the beads in the strong scattering regime. This weak frequency dependence is also shown from calculations of l^* using the SpFA model, where $\langle\cos\theta\rangle$ is determined from the average of $\cos\theta$ weighted by the square of the angle-dependent scattering amplitude (solid curve in fig. 2(c)). Hence the strong frequency dependence of D must be due to the variation of v_E, which was determined experimentally from the ratio $v_E = 3D/l^*$ using the measured values of D and l^*. Figure 2(b) compares the

measurements of the energy velocity with the group velocity, showing that both v_E and v_g, which describe the transport of energy through the sample by diffusive and ballistic waves, respectively, are remarkably similar in magnitude and frequency dependence. This similarity between v_E and v_g, which was not anticipated from earlier theoretical work for light [9], appears to hold quite generally *except* in cases of extreme dispersion, where the group velocity loses its meaning as the ballistic energy transport velocity (even though v_g still describes narrow-band coherent pulse propagation accurately in such extreme conditions). The comparison shown in fig. 2(b) suggests a simple physical picture for v_E and its relationship to v_g. Even in the forward direction, the transport of energy is strongly affected by scattering resonances, which lead to a large scattering delay near the minima in v_g. It is reasonable to expect that wave pulses scattered through a non-zero scattering angle will experience a similar, but not identical, scattering delay, so that in this case v_E should be similar to v_g, with the relation between them taking into account the additional angle-average scattering delay of the scattered waves [4].

These ideas can be formulated quantitatively by extending the SpFA model to calculate the additional scattering delay experienced by a wave pulse. In this approach, the angular dependence of the magnitude and phase shift in a typical scattering event is calculated for each frequency component of the wave pulse from the complex scattering amplitude of the coated elastic sphere embedded in the effective medium. By incorporating these frequency-dependent phase and amplitude variations into the Fourier components of the incident Gaussian pulse, and taking the inverse Fourier transform to recover the scattered pulse, the corresponding time delay of the scattered pulse envelope relative to the forward direction can be calculated for each scattering angle. The intensity-weighted angular average of these additional scattering delays, Δt_{ave}, can then be used to express the energy velocity in terms of the group velocity, giving $v_E = l^*/(l*/v_g + \Delta t_{\mathrm{ave}}) = v_g/(1-\delta_m)$, where $\delta_m = \Delta t_{\mathrm{ave}} v_g/l^*$. Note that, in this approach, v_E, l^*, v_g and δ_m are all calculated in a renormalized effective medium, which accounts for the effects of the multiple scattering that become especially pronounced for high volume fractions of scatterers. Excellent quantitative agreement between the predictions of this model and the experimental data was found not only v_E and l^* but also for the diffusion coefficient that is calculated from them using $D = v_E l^*/3$.

In summary, these ultrasonic experiments in a model system consisting of glass beads in water have enabled a quantitative and comprehensive assessment of the applicability of the diffusion approximation to the description of energy transport by multiply scattered acoustic waves. By comparing the parameters that govern diffusive and ballistic transport over a wide frequency range, a unified physical picture of energy transport in strongly scattering media has emerged. In addition, the success of the SpFA model in describing the experimental results for both ballistic and diffusive waves highlights the relevance of an effective medium description even in the strongly scattering intermediate frequency regime. The methods developed in this work have facilitated both the search for ultrasonic wave localization in more strongly scattering samples (see paper II, this volume, p. 95) and the development of novel dynamic probes of multiply scattering materials (see paper III, this volume, p. 115).

3. – Wave transport in ordered media: phononic crystals in 2D and 3D

The character of ultrasound transport in strongly scattering media is changed dramatically when the scatterers are arranged in an ordered array to form a phononic crystal. These materials are the acoustic and elastic counterparts of photonic crystals for light, and have been the subject of increasing interest since the early 1990s [21]. Because it is relatively easy to control the strength of the scattering contrast between the component materials, phononic crystals may be viewed as ideal media in which to study the profound effects of lattice structure on wave propagation. Much of the initial research concentrated on phononic band gaps, which occur due to Bragg scattering when the wavelength is comparable to the lattice constants, leading to frequency bands where wave propagation is forbidden. As a result, much is now known about the conditions under which phononic crystals with compete band gaps can be fabricated, allowing wave transport in this frequency range to be investigated and novel acoustic waveguides and noise blocking devices to be constructed [22, 23, 24, 25, 26, 27, 28, 29, 30]. Methods for making compact phononic crystal sound insulators have also been proposed and demonstrated [25]. More recently, attention has turned to wave transport in the pass bands both below and above the band gaps, where unusual negative refraction, diffraction and focusing effects have been observed [31, 32, 33, 34, 35].

To illustrate the main differences between ultrasonic wave transport in ordered and disordered structures, consider the results that have been obtained for 3D phononic crystals made from 0.8-mm-diameter tungsten-carbide beads surrounded by water [28, 31]. In this case, excellent crystal quality was assured by the availability of extremely monodisperse spheres due to the needs of the ballpoint pen industry, and meticulous hand-assembly of the spheres in a custom-made mould. In transmission, multiple scattering from the periodic array of scatterers leads to a transmitted pulse in the far field with a well defined, but *coherent*, coda, so that the *entire* transmitted pulse can be analysed by the methods outlined in section **2**.1. Thus, ultrasonic pulsed techniques can readily measure all the basic wave properties of the crystal, including the transmission coefficient (from the ratio of the amplitudes of the FFTs of the transmitted and incident pulses) and the band structure (from the phase shift at each frequency in the pulse, yielding the variation of ω with $k = \Delta\phi/L$).

Typical results for the 3D tungsten-carbide/water crystal can be found in fig. 5. The left pair of panels shows the transmission coefficient and the band structure of this face-centred-cubic crystal, revealing a wide band gap due to Bragg scattering near 1 MHz (width $\sim$ 20% of the central frequency), where the spacing between layers of the crystal is approximately equal to half the wavelength in water. In the [111] direction, in which the experimental data were obtained, the gap is even wider, as shown by the broad dip in the transmission coefficient, measured for a crystal consisting of 12 layers. These results illustrate the relative ease with which wide band gaps can be obtained in acoustics relative to optics, because of the large scattering contrast that can be achieved in ultrasound (for this combination of solid spheres and liquid matrix, the longitudinal impedance ratio is 60). Even wider gaps ($\sim$ 100%) are found in solid-solid systems such

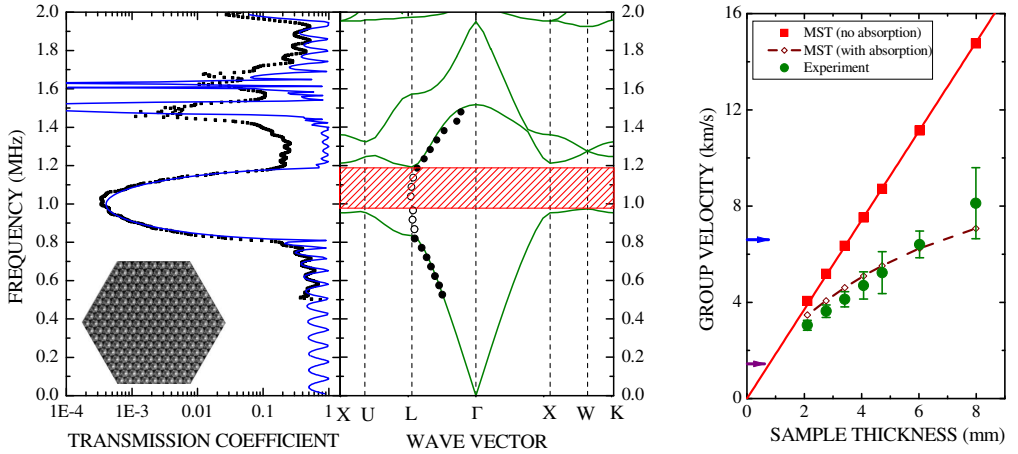

Fig. 5. – left panels: Amplitude transmission coefficient along the [111] direction for a 12-layer fcc phononic crystal made from tungsten carbide beads, and the corresponding band structure. Experimental data are shown by the symbols, and the results of MST calculations by the solid curves. A photo of part of the surface of the crystal is shown in the insert on the left. Right panel: Thickness dependence of the group velocity at a frequency of 0.95 MHz in the first band gap.

as steel beads in epoxy, where coupling with a resonance of the spheres enhances the band gap considerably [29, 36]. In fig. 5 the experimental data are compared with predictions of Multiple Scattering Theory (MST, indicated by the solid curves) [24], which is ideally suited to calculating the properties of phononic crystals built from scattering elements having simple geometric shapes such as spheres, where the scattering can be calculated accurately with no adjustable parameters. Excellent agreement between theory and experiment is found. Note that this agreement indicates that the band structure, which is calculated for an infinite crystal, can be accurately measured by transmission experiments in finite-thickness samples consisting of remarkably few layers.

The transmission coefficient in the middle of the gap (at $f = 0.95$ MHz) is found, both experimentally and theoretically, to decrease exponentially with thickness as $\exp(-\kappa L)$, consistent with evanescent modes having imaginary wave vector κ. This suggests that ultrasound is transmitted through the crystal by tunneling, whose dynamics can be investigated through measurements of the group velocity [28]. The right panel of fig. 5 shows that the group velocity increases linearly with sample thickness, an unusual result that is the classic signature of tunneling, implying that the tunneling time is independent of thickness. For the thickest crystals, the magnitude of v_g is remarkably fast - see the horizontal arrows in the figure for the longitudinal velocities in the two constituent materials. The solid and dashed curves in the figure are calculated using Multiple Scattering Theory both without and with absorption, the latter being taken into account by complex moduli of the constituents. It can be seen that the theory with absorption

gives a very satisfactory description of the experimental results, indicating how dissipation, which has no counterpart in the quantum tunneling case, significantly affects the measured tunneling time. This effect was interpreted using a so-called two modes model, which allows the role of absorption to be understood in simple physical terms [28]. Absorption in the band gap of a phononic crystal cuts off the long multiple scattering paths, making the destructive interference that gives rise to the band gap incomplete. As a result, a small-amplitude propagating mode is produced in parallel with the dominant tunneling mode, accounting for the reduction in the measured group velocity relative to the predictions without absorption. This simple model was also found to give a good quantitative explanation of the data [28].

Experiments on the same 3D tungsten-carbide/water phononic crystal were the first to demonstrate ultrasound focusing by negative refraction [31] - another area of phononic (and photonic) crystal research that is currently attracting considerable attention. At frequencies in the pass band near 1.6 MHz in fig. 5, the initially diverging beam from a quasi-point source was observed to be sharply focused in a plane that was quite far from the crystal, where the focal spot could be easily measured. As is explained in more detail below, focusing occurs because the group velocity inside the crystal is of opposite sign to the wave vector, and as a result the direction of energy transport (which is given by the group velocity) corresponds to a negative angle of refraction. In terms of a simple ray picture, in which the rays are drawn parallel to the group velocity, the wave vector components of the field from the source that are incident at angles $\pm\theta$ are refracted negatively as they enter the crystal, cross inside the crystal and are then refracted negatively again as they leave the crystal, so that the emergent rays converge to to a focus on the far side of the crystal. The data in these initial experiments were interpreted using a Fourier imaging model that accounted for this unusual wave transport through the crystal, giving a quantitative explanation of the observed focusing effect [31].

To explore the phenomena of negative refraction and focusing in phononic crystals in more detail, a number of experiments and theoretical calculations have been performed on 2D crystals [32, 33, 34, 35]. The most direct observations of negative refraction were made by Sukhovich *et al.* [34], who constructed a prism-shaped phononic crystal of steel rods, arranged in a triangular lattice at a volume fraction of 58% and surrounded by water. This crystal has the advantage of a relatively simple band structure, as shown by the solid curves (MST) and symbols (experiment) in fig. 6(a). The second pass band, between the stop band along ΓM (the [1,1] direction) and the band gap near 1 MHz, has a single branch, which appears quite isotropic. This isotropic behaviour is confirmed by the equifrequency contours (fig. 6(b)), which characterize the variation with direction in the magnitude of the wavevector at a given frequency. The contours are remarkably circular and shrink in radius as the frequency increases, indicating that the wave vector has the same magnitude in all directions, and that the group velocity, $\vec{v}_g = \nabla_{\vec{k}}\omega(\vec{k})$, points towards the centre of each circular contour. Thus, for this band, the group velocity and wave vector in the first Brillouin zone are antiparallel for all directions of propagation, a situation resembling left-handed behaviour in negative index metamaterials [37]. A consequence of v_g and k being antiparallel is that waves arriving

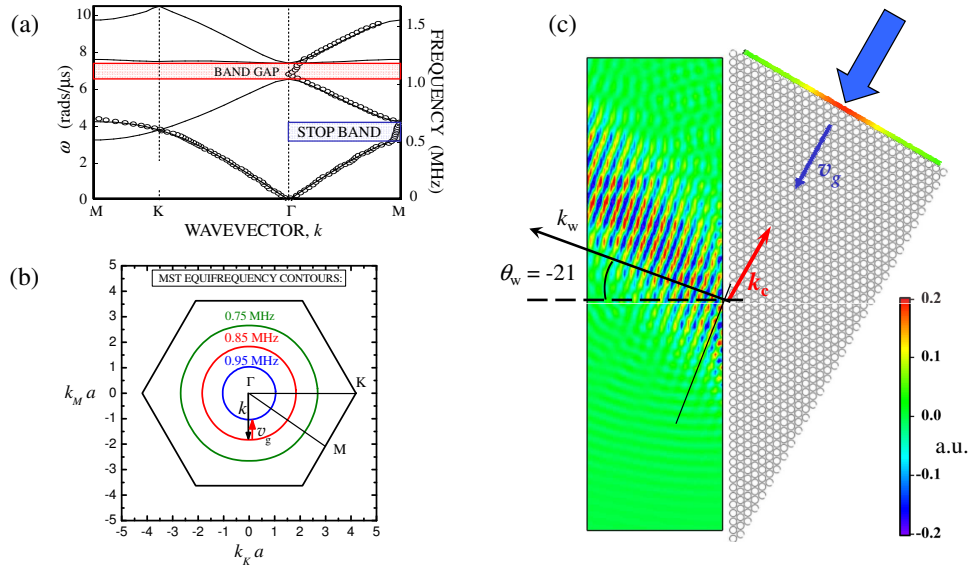

Fig. 6. – (a) Band structure of a phononic crystal of steel rods in water (triangular lattice of 1.02-mm-diameter rods with lattice constant $a = 1.27$ mm). The solid curves were calculated using Multiple Scattering Theory calculations, and the symbols represent experimental data. (b) Equifrequency contours at the three frequencies, 0.75, 0.85 and 0.95 MHz, in the second pass band. (c) Snapshot the negatively-refracted pulse emerging from a phononic crystal prism (angles 30°, 60° and 90°, as shown) after a narrow-band pulse (central frequency of 0.85 MHz) was normally incident on the shortest face of the prism (in the direction of wide blue arrow). The data were measured by scanning a hydrophone in a rectangular grid, digitally filtering the pulses to narrow the bandwidth, and measuring the wave field at a particular moment in time to construct the spatial variation of the field at that time.

at the surface of the crystal at non-normal incidence will be negatively refracted. This effect is demonstrated by the experimental data shown in fig. 6(c), which was obtained by directing a narrowband pulse with central frequency 0.85 MHz towards the shortest face of the prism at normal incidence (see the wide blue arrow) and imaging the field that emerged from the longest face using a miniature hydrophone. Since the wave pulse enters the crystal at normal incidence, the pulse continues to travel inside the crystal in the original direction, which is parallel to the group velocity. As the pulse leaves the crystal, the outgoing field pattern is seen to bend backwards in the negative direction, showing according to Snell's law that the wave vector inside the crystal must also point in the negative direction, opposite to the direction of the group velocity, as predicted from the equifrequency contour. To emphasize this point, the directions of the Bloch wave vector and group velocity inside the crystal are also shown in fig. 6(c), as well as the direction of the refracted beam outside, which is perpendicular to the wave fronts. (Note that to measure the direction of k, it crucial to measure the wave field and not just the intensity

so that k can be determined from the wave fronts, as the position of maximum intensity in the refracted beam in this pulsed experiment is also influenced by the time the pulse reached the exit surface of the crystal, with the earlier arrivals being closer to the top of the prism and corresponding to the signals on the top left part of the measurement area.) Furthermore, the measured refraction angle is given within experimental uncertainty by Snell's law, using the value of the wave vector inside the crystal predicted by MST, providing additional evidence that the data can be quantitatively described in terms of negative refraction.

The direct observation of negative refraction in this 2D phononic crystal suggests that it is a good system in which to investigate focusing by negative refraction in flat phononic crystal lenses, and in particular to examine the ultimate image resolution that may be possible. For this purpose, a rectangular-shaped six-layer crystal of steel rods with the same crystal structure was constructed. Each layer contained 60 rods (to avoid edge effects), and the layers were stacked in the ΓM direction, i.e. with the base of the triangular unit cell parallel to the surface. To explore the resolution capabilities of the lens, a narrow line source (width 0.55 mm, which is less than the wavelength in water at the frequencies of interest) was built from piezoelectric polymer strips. When the crystal was filled and surrounded by water, the best image of the source was measured at 0.70 MHz, the lowest frequency at which the equifrequency contours are circular. However, the image resolution, as determined by the Rayleigh criterion (resolution equals half the full width of the peak Δ, i.e., the distance $\Delta/2$ from the maximum to the adjacent minimum (zero)), was only 1.15λ, where λ is the ultrasonic wavelength in water. This is not as good as the diffraction limit of $\lambda/2$, which is obtained when all propagating components of the field from a point source are brought to focus in the image plane, because the equifrequency contours inside and outside the crystal were not matched, cutting off all angles of incidence greater than 56.8° in this case. To overcome this limitation, a second crystal was built with thin transparent walls to enable the liquid inside the crystal to be replaced by methanol, which has a lower sound velocity than water, shrinking the frequency axis of the dispersion curve by 74%. As a result, the size of the equifrequency contours of both the crystal and the water outside were perfectly matched at a frequency of 0.55 MHz in the second band. Thus, all angle negative refraction (AANR) is achieved at this frequency, and all others down to the bottom of the band at 0.50 MHz. The image obtained at 0.55 MHz, when the source was placed 1.6 mm from the opposite surface of the crystal, is shown in fig. 7(a). A good focal pattern is clearly seen, with the focal spot narrowly confined both perpendicular and parallel to the crystal surface. By fitting a sinc function (fig. 7(b)), the transverse width of the image was measured to be 3.0 mm, with a corresponding resolution of 0.55λ. This shows that a flat phononic crystal with equifrequency contours matched to those of the medium outside is capable of producing images with an excellent resolution approaching the diffraction limit [34].

To achieve super resolution (better than the diffraction limit), it is necessary to capture and amplify evanescent waves from the source - something that clearly did not occur for the data shown in fig. 7(a). However, when the source was brought even closer to the surface of the crystal, 0.1 mm or $\lambda/25$ away, it was found that significantly improved

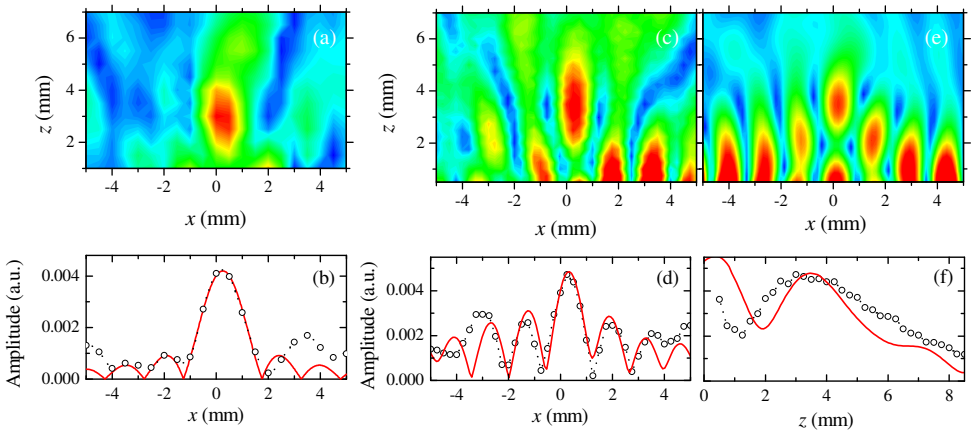

Fig. 7. – Contour maps of the ultrasonic amplitude (magnitude of the FFT of the wave field at the frequencies indicated) on the imaging side of a flat methanol-steel phononic crystal lens for a 0.55-mm-wide line source, and corresponding plots of the amplitude through the focus. (a): Image measured at 0.55 MHz for a source-lens distance of 1.6 mm. (b): Amplitude parallel to the lens surface (circles) through the focus in (a). The data are compared with a sinc function (red line), indicating a resolution $\Delta/2 = 0.55\lambda$. (c) and (e): Images measured (c) and calculated with FDTD (e) for a frequency of 0.53 MHz when the source-lens distance is only 0.1 mm. Note the appearance of a bound mode of the crystal, which decays evanescently as the distance from the surface (at $z = 0$) increases. (d) and (f): Comparison of experiment (circles) and theory (solid curves) for the transverse width of the focal spot (d) and its variation with distance from the surface of the crystal (f). Super resolution is evident from the half widths of the primary peaks in (d), give a resolution of 0.37λ and 0.35λ for experiment and theory, respectively.

resolution could be obtained [35] . The best resolution was found at a slightly lower frequency, 0.53 MHz, as shown by the experimental results in figs. 7(c)(d) and (f), which are compared with Finite Difference Time Domain (FDTD) simulations in figs. 7(d)-(f). Both the experimental and theoretical resolutions, 0.37λ and 0.35λ, are clearly better than the diffraction limit. The reason why super resolution can be attained for this very small source-crystal separation is that some of the evanescent waves from the source are now able to couple to a bound mode of the crystal, and hence become amplified sufficiently to participate in image restoration. Evidence for the excitation of this bound mode can be seen in the field patterns of figs. 7(d) and (e), which show several subsidiary peaks that are largest at the crystal surface; these additional peaks (not seen in (a)) decay rapidly with distance from the crystal, as expected for the evanescent decay of bound crystal modes. Additional evidence for the existence of this bound mode was obtained from FDTD calculations of the band structure of a finite crystal slab with the same number of layers as in the experiment. These calculations revealed a nearly flat band that extends from 0.525 MHz at the water to 0.51 MHz at the zone boundary; as it lies below the water line, this mode is bound to the crystal slab as it cannot propagate in water. The best focusing is seen at 0.53 MHz, as this frequency lies between the frequency for

perfectly matched equifrequency contours (0.55 MHz) and the resonance frequencies of the bound mode (0.51 - 0.525 MHz), but is still close enough to the bound mode that it can be excited. Calculations of the field patterns inside the phononic crystal indicate that this bound mode is a slab mode of the crystal, and not a surface mode.

This demonstration that super resolution can be achieved in practice with phononic crystal lenses is enabling a detailed study of the many factors that can influence the optimum resolution. Perhaps the most interesting question concerns the mechanism that sets the resolution limit for this crystal. This is determined by the largest transverse wave vector k_{max} that the crystal will support, with the most logical choice for k_{max} being the wave vector at the Brillouin zone boundary of the crystal along the ΓK direction (parallel to the surface of the lens). (Note that since the bound mode that is excited is a slab mode of the crystal, it is the bulk Brillouin zone boundary and not the surface Brillouin zone boundary that sets the resolution limit, allowing better resolution to be achieved for this triangular lattice than would be found for the surface modes that were considered by Luo et al. for photonic crystals.) This condition gives $k_{\max} = 4\pi/3a$. If we assume perfect transmission for all transverse wave vectors $k_\perp$ less that $k_{\max}$, and zero transmission for $k_\perp$ greater than $k_{\max}$, then the image amplitude will vary with distance x parallel to the crystal surface as $\left|\int_{-k_{\max}}^{k_{\max}} \exp[ik_\perp x]dk_\perp\right| = |2\sin(k_{\max}x)/(k_{\max}x)|$ so that the resolution limit $\Delta_{\min}/2 = \pi/k_{\max} = 3a/4$. This condition gives $\Delta_{\min}/2 = 0.34\lambda$ at 0.53 MHz, which is very close to our experimental and FDTD results.

In conclusion, these experimental and theoretical results demonstrate the conditions needed to achieve optimal focusing: (i) the equifrequency surfaces/contours should be spherical/circular, (ii) the equifrequency surfaces in the phononic crystal and in the medium outside should be matched, and (iii) the crystal should have a bound mode at a frequency close to the operational frequency, in order to enable amplification of evanescent waves from the source, for super resolution to be attained. The analysis of the maximum possible resolution that can be obtained with the 2D methanol-steel phononic crystal will be useful for designing new phononic crystal lenses in which the super resolution may be enhanced.

4. – Conclusions

Experiments with ultrasonic waves are playing an increasing important role in probing and understanding the rich diversity of wave phenomena that occur in strongly scattering media. In disordered media, the phase sensitivity of ultrasonic detectors enables pulsed experiments to separate the coherent, forward-scattered signal, which propagates ballistically through the medium, from the multiply scattered coda. Thus, transmission experiments can be used to obtain a very complete set of measurements of wave transport through the medium, allowing the parameters that describe both ballistic and diffusive propagation to be compared over a wide frequency range. Such measurements have been performed on a simple model system of glass beads in water, illustrating the potential of ultrasound for gaining useful insights into the character of wave transport in the presence of strong multiple scattering, and laying a useful foundation for future experiments on

more complex systems.

In the second part of this paper, the properties of ordered acoustic media, or phononic crystals, have been reviewed. The main emphasis has been on focusing by negative refraction, where super-resolution imaging has recently been demonstrated experimentally. This area of research continues to grow, providing complementary information and applications to analogous optical experiments on photonic crystals.

* * *

I would like to thank the many students and colleagues who have contributed to the research that has been reviewed in this paper. Support from NSERC is also gratefully acknowledged.

REFERENCES

[1] Sheng P., *Introduction to Wave Scattering, Localization and Mesoscopic Phenomena* (Academic Press, San Diego) 1995.
[2] Page J.H., Schreimer H.P., Bailey A.E. and Weitz D.A., *Phys. Rev. E*, **52** (1995) 3106.
[3] Page J.H., Sheng P., Schreimer H.P., Jones I., Jing X. and Weitz D.A., *Science*, **271** (1996) 634.
[4] Schreimer H.P., Cowan M.L., Page J.H., Sheng P., Liu Z. and Weitz D.A., *Phys. Rev. Lett.*, **79** (1997) 3166.
[5] Cowan M.L., Beaty K., Page J.H., Liu Z. and Sheng P, *Phys. Rev. E*, **58** (1998) 6626.
[6] Faez S., Johnson P.M. and Lagendijk A., *Phys. Rev. Lett.*, **103** (2009) 053903.
[7] Sommerfeld A., *Ann. Phys.*, **44** (1914) 177.
[8] Brillouin L., *Wave Propagation and Group Velocity* (Academic Press, New York) 1960.
[9] van Albada M.P., van Tiggelen B.A., Lagendijk A. and Tip A.P., *Phys. Rev. Lett.*, **66** (1991) 3132.
[10] Liu J., Ye L., Weitz D.A. and Sheng P., *Phys. Rev. Lett.*, **65** (1990) 2602.
[11] Leighton T.G., *The Acoustic Bubble* (Academic Press, San Diego) 1994.
[12] Leroy V., Strybulevych A., Page J.H. and Scanlon M.G., *J. Acoust. Soc. Amer.*, **123** (2008) 1931.
[13] Leroy V., Strybulevych A., Scanlon M.G. and Page J.H. , *Euro. Phys. J.*, **29** (2009) 123.
[14] Leary D., de Bruyn J.R. and Page J.H., *Bull. Am. Phys. Soc.*, **46(1)** (2001) 947.
[15] Chu S. and Wong S., *Phys. Rev. Lett.*, **48** (1982) 738.
[16] Oughstun K.E. and Sherman G.C., *Electromagnetic Pulse Propagation in Causal Dielectrics* (Springer-Verlag, Berlin) 1994.
[17] Zhang Z.Q., Jones I.P., Schreimer H.P., Page J.H., Weitz D.A. and Sheng P., *Phys. Rev. E*, **60** (1999) 4843.
[18] Weaver R.L. and Sachse W., *J. Acoust. Soc. Am.*, **97** (1995) 2094.
[19] Tourin A., Derode A., Roux P., van Tiggelen B.A. and Fink M., *Phys. Rev. Lett.*, **79** (1997) 3637.
[20] Durian D.J., *Phys. Rev. E*, **50** (1994) 857.
[21] Psorobas I.E., (ed.) *Phononic Crystals: Sonic bandgap materials*, a special issue of *Zietschrift für Kristallographie*, **220** (2005) .

[22] Economou E.N. and Sigalas M.M., *Phys. Rev. B*, **48** (1993) 13434; *J. Acoust. Soc. Am.*, **95** (1994) 1734.
[23] Kushwaha M.S., Halevi P., Dobrzynski L. and Djafari-Rouhani B., *Phys. Rev. Lett.*, **71** (1993) 2022; Kushwaha M.S., Djafari-Rouhani B., Dobrzynski L. and Vasseur J.O., *Eur. Phys. J. B*, **3** (1998) 155.
[24] Kafesaki M. and Economou E.N., *Phy. Rev. B*, **60** (1999) 11993; Psarobas I.E., Stefanou N. and Modinos A., *Phys. Rev. B*, **62** (2000) 278; Liu Z., Chan C.T., Sheng P., Goertzen A.L. and Page J.H., *Phys. Rev. B*, **62** (2446) 2000.
[25] Liu Z., Zhang X., Mao Y., Zhu Y.Y., Yang Z., Chan C.T. and Sheng P., *Science*, **289** (2000) 1734.
[26] Torres M., Montero de Espinosa F.R. and Aragn J.L., *Phys. Rev. Lett.*, **86** (2001) 4282.
[27] Vasseur J.O., Deymier P.A., Chenni B., Djafari-Rouhani B., Dobrzynski L. and Prevost D., *Phys. Rev. Lett.*, **86** (2001) 3012.
[28] Yang S., Page J. H., Liu Z., Cowan M.L., Chan C.T. and Sheng P., *Phys. Rev. Lett.*, **88** (2002) 104301.
[29] Page J.H., Yang S, Liu Z., Cowan M.L., Chan C.T. and Sheng P., *Zietschrift für Kristallographie*, **220** (2005) 859.
[30] Mei J., Liu Z., Shi J. and Tian D., *Phys. Rev. B*, **67** (2003) 245107.
[31] Yang S., Page J.H., Liu Z., Cowan M.L., Chan C.T. and Sheng P., *Phys. Rev. Lett.*, **93** (2004) 024301.
[32] Zhang X. and Liu Z., *Appl. Phys. Lett.*, **85** (2004) 341.
[33] Ke M., Liu Z., Cheng Z., Li J., Peng P. and Shi J., *Solid State Comm.*, **142** (2007) 177 .
[34] Sukhovich A., Jing L. and Page J., *Phys. Rev. B*, **77** (2008) 014301.
[35] Sukhovich A., Merheb B., Muralidharan K, Vasseur J.O., Pennec Y., Deymier P.A. and Page J.H., *Phys. Rev. Lett.*, **102** (2009) 154301.
[36] Sainidou R., Stefanou N. and Modinos A., *Phys. Rev. B*, **66** (2002) 212301
[37] Pendry J.B., *Phys. Rev. Lett.*, **85** (2000) 3966.
[38] Luo C., Johnson S.G., Joannopoulos J.D. and Pendry J.B., *Phys. Rev. B*, **68** (2003) 045115.